Universidad de Valladolid

FACULTAD DE CIENCIAS

TRABAJO FIN DE MÁSTER

Máster en Nanociencia y Nanotecnología Molecular

TRANSPARENT NANOCELLULAR POLYETHERIMIDE

Autor:

Félix Lizalde Arroyo

Tutoras:

Dra. Judith Martín de León

Dra. Victoria Bernardo García

Año:

2023

Resumen en español

Se ha fabricado polieterimida (PEI) nanocelular y transparente con densidad relativa en torno a 0.7 utilizando la técnica de espumado denominada *"espumado por disolución de gas*, o *"gas dissolution foaming"* en inglés. Se ha evaluado el efecto de las condiciones de proceso y se ha llevado a cabo la caracterización completa de estos materiales en este trabajo. Se han estudiado dos líneas de trabajo diferentes en función del parámetro de saturación (temperatura o presión) que se mantuviera constante. En primer lugar, para una temperatura de saturación constante (24ºC) se han saturado las muestras a 5.5, 10 y 20 MPa (las presiones de saturación más altas de la literatura). Por otro lado, se ha mantenido la presión constante (5.5 MPa) para saturar las muestras a 24, 0 y -10 ºC. De esta manera se ha podido estudiar cómo afectan estos parámetros a la solubilidad obteniendo el valor más alto en un 18% de CO_2 en la muestra saturada a -10 ºC y 5.5 MPa. Gracias a que se han obtenido altos valores de solubilidad, se han conseguido valores de densidad de nucleación de 10^{15} a 10^{16} núcleos/cm^3 y tamaños de celda por debajo de los 50 nm además de una estructura muy homogénea. Estas nanoestructuras han permitido obtener materiales con una transparencia de hasta casi el 0.90 para el color rojo y para un espesor de 0.5 mm.

Abstract

Nanocellular transparent polyetherimide (PEI) with relative density around 0.7 has been produced using the so-called *gas dissolution foaming* technique. The relationship between the production parameters, the obtained cellular structure, and the transparency of the produced cellular materials has been stablished. Two parallel studies were conducted depending on the saturation parameter (temperature or pression) held constant. Firstly, for a constant saturation temperature (24 ºC), the samples were saturated at 5.5, 10 and 20 MPa (the highest saturation pressures ever used in the literature). On the other hand, the pressure was kept constant (5.5 MPa) to saturate the samples at 24, 0 and -10 ºC. In this way, it was possible to study how these parameters affect solubility, obtaining the highest value of 18% CO_2 in the sample saturated at -10 ºC and 5.5 MPa. Thanks to the high solubilities achieved in these saturation processes, cell nucleation density values of 10^{15} to 10^{16} nuclei/cm^3 and cell sizes below 50 nm have been obtained, as well as a very homogeneous structure. These nanostructures have made it possible to obtain materials with a transparency of up to almost 0.90 for the red colour at a thickness of 0.5 mm.

Table of content

1. Introduction

The development and evolution of materials have always been driven by several reasons. These include the need to solve various problems that have arisen in society, or the search for materials that outperform existing ones. As a result, the design of polymeric materials has progressed enormously in recent years. Polymers are materials characterised by a molecular structure formed by the repetition of a structural unit called a monomer. The properties of these materials depend to a large extent on the nature of their monomers and the way in which they are organised[1,2]. These materials combine many good properties such as good mechanical strength to density ratio, high resistance to chemicals or low production cost[3]. Although they are widely used in industry and science, these materials have certain weaknesses that need to be considered for their different applications. Some of these weaknesses are their low resistance to high temperatures or flames or their degradation by exposure to UV radiation, among other things[2]. In addition, despite having a good mechanical strength to density ratio, other materials such as metals show a very good performance in these fields.

As a result of these shortcomings, the so-called high-performance polymers[4] have emerged. These unlike common polymers are noted for their low density, high thermal stability, chemical resistance, and high mechanical strength. In several high-performance applications, such as the automotive, aerospace, electronics, energy and medical sectors, their molecular structure and characteristics are specially engineered to meet stringent standards. Due to the complexity of their synthesis and the need for high quality raw materials, high performance polymers are generally more expensive to manufacture[4,5]. Although the properties of these high-performance polymers are already very good, it is important to keep improving and develop new and better materials, as technological challenges require constantly outstanding performance. One way to provide different properties to polymers is to incorporate a cellular structure into them.

Cellular polymers are two-phase systems in which one of the phases is a gas dispersed in a continuous polymer matrix[6,7]. These materials present different properties than their former solid with a reduction of their weight, raw material, and cost, together with properties such as low thermal conductivity, low density, buoyancy, etc. Thanks to this, they have a strong presence and even greater future projection in relevant technological sectors such as the automotive, renewable energies, construction, packaging, biotechnology and aeronautics, among others[8]. Although there are various cellular materials that can be found in nature in different forms such as cork, coffee grains or bones[9], human beings have developed improved and optimised cellular polymers to adapt them to any of our needs. Throughout the 20th century, cellular polymers have evolved by reducing their cell size (ϕ) from conventional cellular

polymers (100-500 µm), through microcellular polymers (1-10 µm) to the 21st century, which has seen the emergence of nanocellular polymers (<1 µm)[6].

Nanocellular polymers are a promising class of cellular materials. They have attracted a great deal of interest from various companies due to their outstanding properties. These materials are characterised by cell sizes in the nanometre scale as can be seen in Figure 1[8].

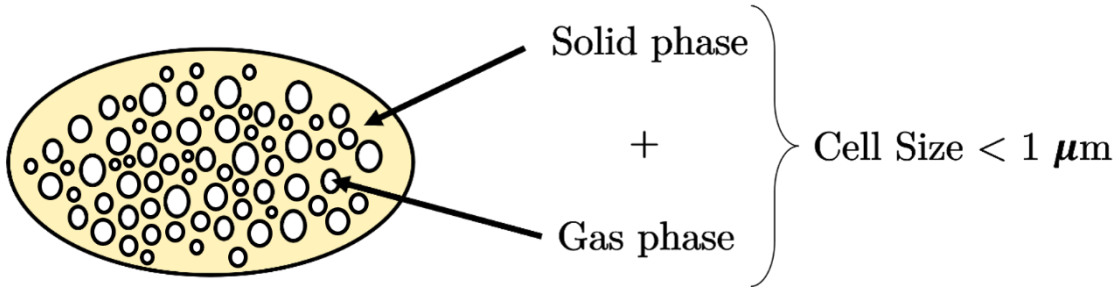

Figure 1. Structure of a nanocellular polymer.

This reduction of the cell size to the nanoscale produces a double confinement effect. The first is in the gas phase. By creating nanometre-sized pores, the gas is confined in an extremely small space. The second is the confinement of the polymer matrix within the thin walls located between the cells, which are also on the nanometric scale. These effects give nanocellular polymers very interesting properties. Regarding gas phase confinement, we get the reduction in the gaseous thermal conductivity due to the Knudsen effect[10–12]. This effect consists of reducing the contribution of mass and energy transport by molecular collisions by making gas molecules more likely to collide with the pore walls than with each other, reducing heat transfer through the gas. Although this effect occurs at cell sizes that are smaller than 100 times the mean free path (l_g =70 nm) of air particles ($\phi < 100\, l_g$)[11,13], it becomes more important in nanocellular polymeric materials when the cell size is reduced below the micron. This effect makes these materials suitable for the thermal insulation industry. In terms of the solid phase, the confinement of the polymer can improve mechanical properties and raise the glass transition temperature[14,15]. It is important to emphasise that these properties related to solid phase confinement have only been proven for large reductions in cell size. Some of the mechanical properties that are improved have been investigated in various papers. For example, in 2011, Miller et al.[16] compared the mechanical properties of microcellular polyetherimide (PEI) (4 µm cell size and relative density between 0.75 and 0.9) with nanocellular PEI (40 nm cell size and similar relative density). In their study, they show that strain at break, modulus of elasticity and impact properties are significantly improved by introducing a nanocellular structure. Also in 2019, Martín de León et al.[15] compare microcellular PMMA materials (cell size 1 µm and relative density between 0.37 and 0.53) with nanocellular PMMA (cell sizes from 20 to 84 nm and relative densities like the microcellular materials). In their research, they

observed an improvement in fracture toughness by reducing the cell size to the nanometre scale. In addition, nanocellular polymers can maintain their transparency if they are produced from transparent polymers and if the pore size is lower than 50 nm. When the cell size is much smaller than the wavelength (λ) of the light passing through it, namely $\phi < \lambda_{light} / 10$ (limit in which the scattering mechanism change from Mie to Rayleigh[17,18]), the amount of scattered light significantly reduces allowing for higher light transmission. So, knowing that the visible light spectrum is between 400 and 700 nm, and centred in 500 nm (green colour), if pores with a size smaller than 50 nm are obtained, the cellular material becomes transparent. Combine transparency with the low thermal conductivity and improved mechanical properties of these materials opens the possibility of use them as insulating windows, for example. Moreover, one should not forget other properties of nanocellular materials such as high surface area or the ability to obtain interconnected cells. The combination of all these properties together makes nanocellular polymers with cells below 50 nm an exceptional material with the potential to be used in a wide range of applications that cannot use conventional cellular materials, such as the production of membranes for microfiltration and ultrafiltration, catalysis, and sensors, among others[19].

Manufacturing nanocellular polymers is a challenging process, as unique technologies are needed to create and stabilise the cells produced at the nanoscale such as chemical induction phase separation techniques (CIPS), imprinting or templating approaches[20]. One of the most used foaming techniques to produce big dimension samples (with a thickness above the millimetre) is called *gas dissolution foaming*, which uses physical blowing agents (usually carbon dioxide (CO_2)) and does not require the use of organic solvents or other additional substances[6,7]. The process consists of three steps: saturation, depressurisation, and foaming. Firstly, during saturation step a physical blowing agent is dissolved in a polymer matrix. Saturation parameters, that is, saturation pressure (P_{Sat}) and saturation temperature (T_{Sat}), must be controlled to obtain the required amount of dissolved gas, namely solubility. During depressurization the pressure is fast released at the so-called depressurization velocity allowing phase separation, that means nucleation in the polymer matrix. Finally, in the foaming step, foaming parameters, foaming temperature and foaming time, are controlled to allow cell expansion and to achieve a uniform porous structure. All production parameters influence the characteristics and therefore the physical properties of the resulting foam. This method appears to be the most suitable for the production of large-scale nanocellular polymers[21].

Depending on the type of nucleation process we can talk about homogeneous or heterogeneous nucleation[22]. Heterogeneous nucleation involves the addition of a second phase, such as inorganic particles or another polymeric phase, which controls the nucleation by reducing the energy required to form stable nuclei[6,22]. On the other hand, homogeneous nucleation occurs without the introduction of a

second phase and is the one commonly used to obtain the smallest cell sizes. In this case one of the key parameters to obtain cells in the nanoscale is the solubility, controlled trough the saturation parameters. As the solubility increases the cell size becomes smaller, existing a solubility threshold, that depends on the gas-polymer system, allowing to reduce the cell from the micro to the nanoscale. For this reason, to achieve cell sizes in the nanometric scale the solubility should be maximized normally through using extreme saturation conditions, such as very high pressures, or very low temperatures. The process becomes even trickier to obtain cell sizes below 50 nm, that is the threshold required to achieve transparency. However, such cell sizes have already been obtained in the literature through homogeneous nucleation and by using different matrices, like polycarbonate (PC)[23], poly(methyl-methacrylate) (PMMA)[24,25], or polyetherimide (PEI)[16,26]. Nevertheless, few of these papers deals with the possible transparency of the obtained cellular materials. Martín de León et al.[24] proved the transparent character of PMMA-based nanocellular foams. Solubilities of 48 % obtained through 20 MPa and -32 ºC of saturation conditions are needed to obtain 14 nm cell sizes and transmittance of 64 % (for 0.5 mm in thickness). In a later work and by using 50 MPa and 0 ºC, Martín-de León et al. [18] report solubilities of 45 % leading to 23 nm and transmittances of 61 % (for 0.5 mm in thickness). On the other hand, Guo et al. reported that the needed solubility to obtain 28 nm cell size in polycarbonate (PC) is of 20.4 %, presenting the samples a 20 % of transmittance.

For high performance polymers, however, transparency has not been studied in detailed. Moreover, the manufacture of nanocellular polymers with such materials is relatively scarce. As stated before, cell sizes below 50 nm are required to obtain this property. Thus, data in the literature dealing the manufacturing of high-performance polymers with cell sizes below 50 nm has been searched. Merlet et al.[27] obtain, by thermal decomposition technique, a material based on poly(phenylquinoxaline) (PPQ) with cells below 50 nm (approximately 5 to 25 nm) and relative densities between 0.7 and 0.9. In 2015, Huimin et al.[28] were able to form nano-cells of less than 50 nm in polysulfone (PSU). The cell sizes obtained are between 22 and 36 nm with relative densities between 0.85 and 0.50. In these cases, CO_2 concentrations in the saturated polymer are between 13 and 15 %. Finally, Miller et al.[26] have successfully produced PEI-based nanocellular materials. The saturation conditions used to obtain materials with cell sizes ranging from 30 to 50 nm, are 4 and 5 MPa and 21 °C leading to 10-12 % of CO_2. They obtain relative densities for these materials between 0.55 and 0.70.

As previously discussed, the transparency of high-performance nanocellular polymers is a quite interesting topic with a huge number of possible applications. The aim of this work is to obtain a transparent high-performance nanocellular polymer, obtaining a relationship between the production parameters-cellular structure-optical properties, that would allow us to understand and control the

process. From the previous paragraphs, PEI is one high-performance polymer that needing low solubilities and no extreme production conditions to lead to cells smaller than 50 nm. In addition, PEI is notable for its amber colour, high glass transition temperature, excellent flame retardancy and very good mechanical properties[29–32]. Therefore, in this research we will work on the production of transparent nanocellular materials based on PEI. Different saturation conditions will be used relating them with the solubility of the material, its cellular structure and finally its transparency.

2. Experimental

2.1. Materials

ULTEM™ Resin 1000 - PEI was kindly supplied by SABIC in the form of 1 mm thick injected sheet. This PEI has a melt flow index (MFI) of 16.5 g/10 min (measured at 360 °C and 5 kg), a density (ρ) of 1.27 g/cm3 and a glass transition temperature of 215 ºC measured by Differential Scanning Calorimetry (DSC) (model DSC822e, Mettler) using a heating programme from 100 ºC to 350 ºC at a rate of 20 ºC/min.

Also, the blowing agent used for the gas dissolution foaming technique was carbon dioxide (CO_2) (99.9% purity).

2.2. Precursor materials production

Solid precursors with dimensions of 20 x 20 x 0.5 mm^3 were produced for the foaming tests from the supplied sample with the following procedure. As it can be seen in Figure 2, after drying the material for 24 hours at 60 ºC under vacuum (a), the sheet supplied by SABIC is compressed moulded, placing it between two heavy metal plates and silicone to prevent it from sticking to the plates (b). The structure is then placed in an oven at 375 ºC for 20 minutes to soften the material (c). After this time, the structure is quickly placed in the hot plate press from Remtex (Barcelona, Spain) for 2 minutes at 220 ºC with a pressure of 10 MPa (d). After this time, the structure is placed in the cold plate press to cool down at the same pressure (e). Finally, after removing the material from the structure (f), we select the central area of the resulting material (g) and make 2x2 cm^2 cuts to obtain the solid precursors for the foaming experiments (h). This method reduces the thickness from the initial 1 mm to 0.5 mm. According to Fick's laws of diffusion[33], the diffusion time of gas in a plane-parallel plate is directly proportional to the square of the sample thickness, so if we reduce the thickness of the precursor using the method described above, we will reduce the saturation time of the sample.

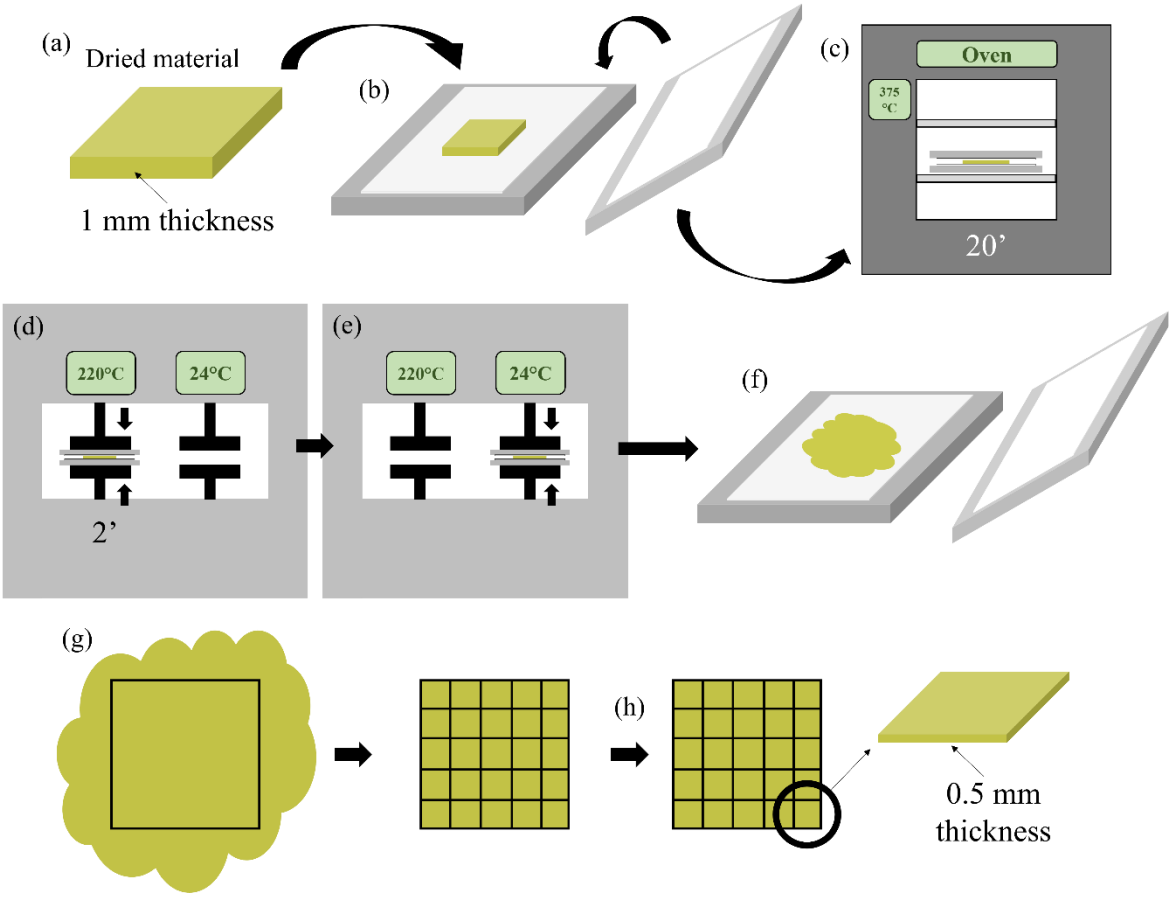

Figure 2. Scheme of the process to obtain PEI solid precursors 0.5 mm in thickness.

2.3. Nanocellular materials production

The manufacturing process of the nanocellular materials was carried out using a pressure vessel as shown in Figure 3 (model High Pressure Chemical Reactor) provided by Supercritical Fluid Technologies with a capacity of 100 millilitres, capable of operating temperatures between −40 °C and 200 °C and a maximum pressure of 69 MPa.

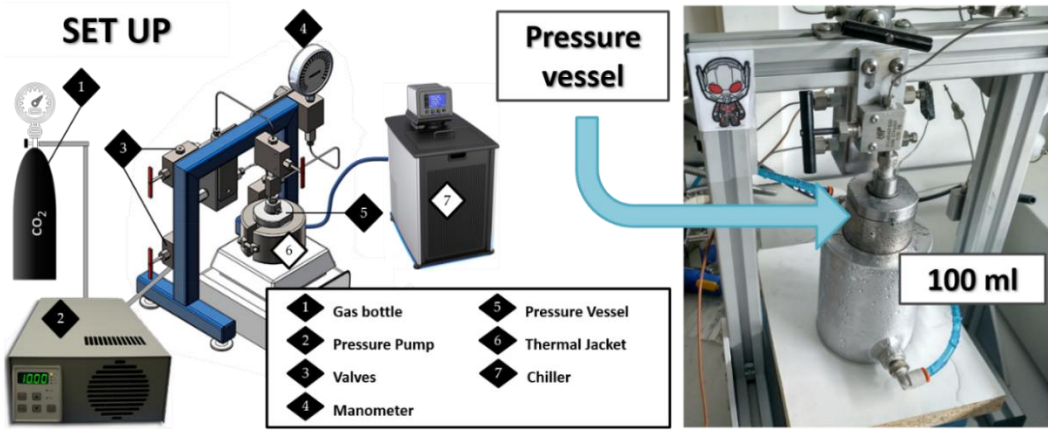

Figure 3. Pressure system set-up[18].

The rest of the equipment used, shown in Figure 3, consists of a pressure pump (2) (model SFT-10 from Supercritical Fluid Technologies), which provides the system with the necessary pressure. The temperature is controlled by a chiller (7) (model AD15R-40-A11B 15L supplied by Polyscience), connected to a thermal jacket (6).

With this configuration, foaming experiments were carried out using the gas dissolution foaming process. First, the samples were introduced into the vessel. For this work, the saturation conditions were varied according to a constant parameter as shown Figure 4. In the first case, keeping a constant temperature of 24 ºC, tests were carried out at 5.5, 10 and 20 MPa. In the second case, maintaining a constant pressure of 5.5 MPa, the tests were conducted at -10, 0 and 24 ºC. Saturation times have been changed accordingly to the production conditions to fully saturate all samples. This way we can analyse the influence of the saturation pressure and the saturation temperature independently. After the saturation process, the pressure was quicky released using a pressure drop rate of 100 MPa/s. The saturated samples were foamed in a silicon thermal bath at 150 °C for 30 s. The desorption time between depressurisation and foaming is 150 s.

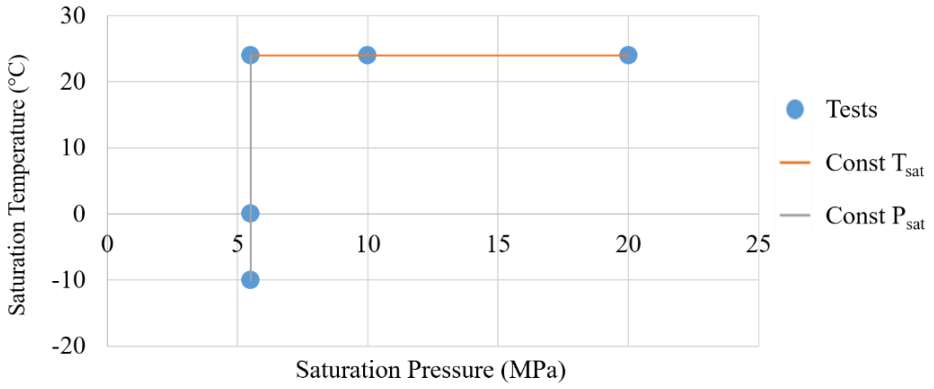

Figure 4. Saturation parameters of the tests carried out in this work.

2.4. Characterization

2.4.1. Solubility

The solubility was calculated as the percentage increase in mass between the initial precursor and the saturated sample. This mass difference is due to the CO_2 dissolved in the polymer matrix and was measured using a Mettler-Toledo balance. To obtain the initial saturation value, as shown in Figure 5, the mass loss must be plotted as a function of the square root of time divided by the thickness (a). For times close to 0 s, the mass loss is linear, so the first values are used to extrapolate the CO_2 concentration value at t = 0 s (b)[18,34].

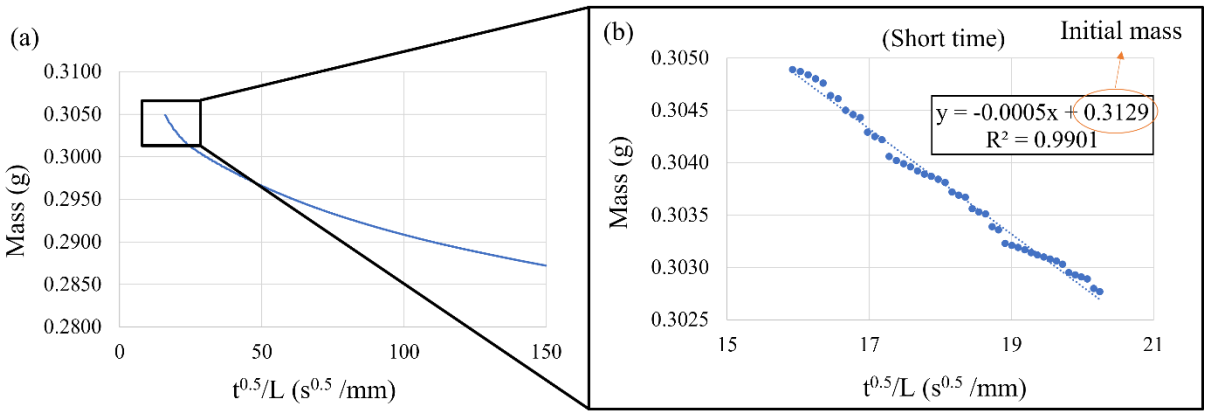

Figure 5. (a) Example of a desorption curve mass vs the square root of time divided by the thickness. (b) Zoom of the first seconds of the desorption curve. Extrapolation of solubility for time 0 s.

2.4.2. Density

The density of both solid PEI (ρ_s) and PEI-based nanocellular materials (ρ_f) was determined using the water displacement method based on Archimedes' principle. A Mettler-Toledo AT261 balance was used in conjunction with a density determination kit. The nanocellular materials density (ρ_f) were measured after a period of time to ensure that all the CO_2 had completely diffused out from the interior and after washing with soap and water to remove all the silicone after foaming. The relative density (ρ_r) is calculated as the ratio of the two measured densities ($\rho_r = \rho_f/\rho_s$)[18].

2.4.3. Structure

A Scanning Electron Microscope (QUANTA 200 FEG, Hillsboro, OR, USA) was used to visualise the nanocellular structure. Samples were prepared for characterisation. First, they were fractured under liquid nitrogen, to keep the nanocellular structure intact. They were then iridium coated using a sputter

coater (model SDC 005, Balzers Union, Balzers, Liechtenstein). The micrographs obtained by ESEM were carefully analysed using ImageJ/FIJI based software[18,35], obtaining different structural parameters of the nanocellular materials. Firstly, the average cell size in 3D is obtained geometrically after counting between 150 and 300 cells per material. The results are presented together with their standard deviation (SD) to give an idea of the homogeneity of the measured structure. In addition, the parameter (SD/ϕ) (normalised standard deviation coefficient) is presented to provide a value of the homogeneity of the cellular structure. If this value is close to 0, it represents a homogeneous structure with little variation in cell size. The cell density (N_v) was determined by Kumar's method[36], applying equation (1) where *A* is the examined area and *n* is the number of cells in that area.

$$N_v = \left(\frac{n}{A}\right)^{\frac{3}{2}} \quad (1)$$

Finally, the number of nucleation points per cubic centimetre of solid material is obtained. This quantity can be calculated from the foam cell density (equation (1)), assuming that each nucleation point in the solid is converted into a cell, thus neglecting the possible effects of degeneration of the cell structure.

$$N_0 = \frac{N_v}{\rho_r} \quad (2)$$

2.4.4. Transmittance

The system used to measure transmittance consists of a light source and a detector as it can be seen in Figure 6. The detector is based on a photodiode inside an integrating sphere with a 12.5 mm window (PRW0505, Gigahertz-Optik) connected to a photometer (X94, Gigahertz-Optik). Three lasers with wavelengths of 650 nm (red), 532 nm (green) and 450 nm (blue) act as light sources. To determine the transmitted intensity, the samples are placed in contact with the window of the integrating sphere to collect all the transmitted light.

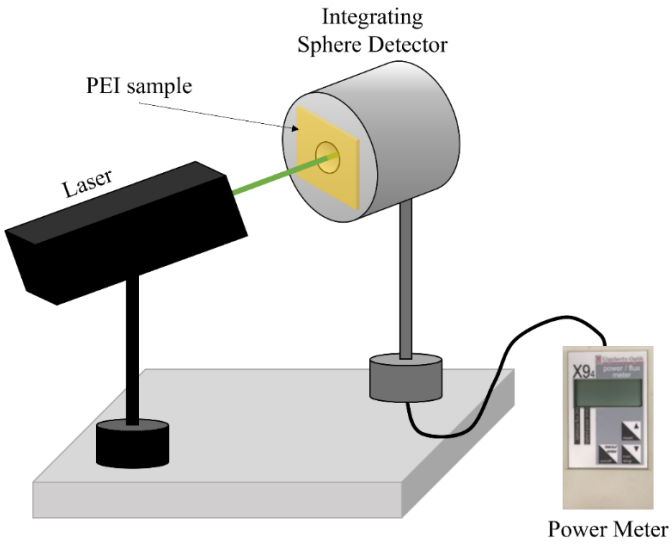

Figure 6. Transmittance system set-up.

Transmittance is determined as the ratio of the intensity passing through a material (I) to the initial intensity (I_0), ($T = I/I_0$)[17,18,24]. The transmittance of the nanocellular materials has been normalised with respect to the one of the solid precursors (T_n) (the transmittance of the solid PEI precursor is 0.92 for the red wavelength, 0.89 for the green wavelength and finally 0.68 for the blue wavelength).

In order to compare the measurement between all samples, the value obtained was also normalised to the thickness of each sample using the following relationship[18], which represents the equation (3).

$$T_n = T_{n0}^{\frac{l}{l_0}} \tag{3}$$

Where T_{n0} is the transmittance measured for the thickness of the sample, l_0, and T_n is the transmittance for a different thickness, l. The Beer-Lambert law, tested in a previous work for PMMA[17], serves as the basis for this relationship. For comparison, the transmittance of all samples produced was calculated for a thickness of 0.5 mm.

3. Results and discussion

3.1. Precursor materials

3.1.1 Solubility

Figure 7 shows the dependence of the solubility with the saturation pressure and saturation temperature.

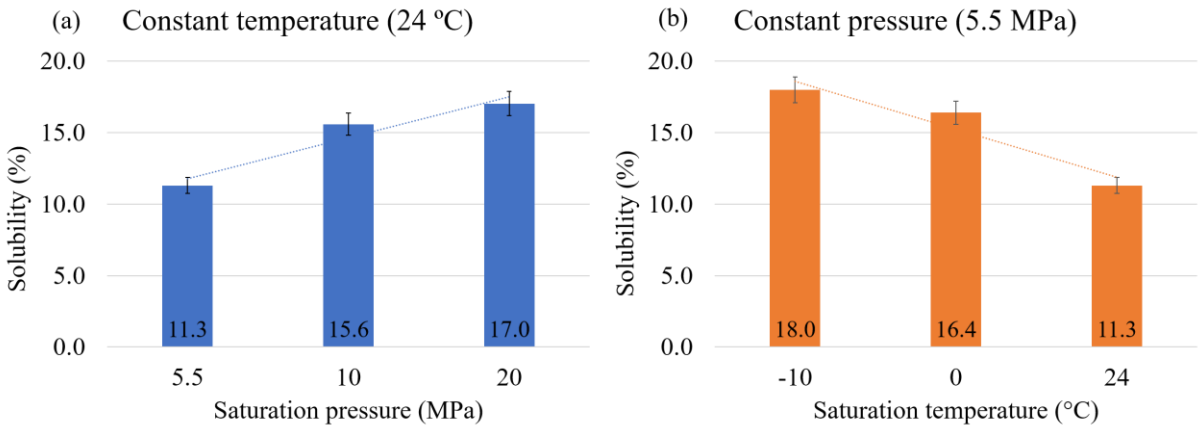

Figure 7. Solubility of samples as a function of saturation pressure at 24°C of saturation temperature (a) and as a function of saturation temperature at 5.5 MPa of saturation pressure (b).

Two different trends can be observed depending on which parameter is held constant. When the saturation temperature is constant (24 °C), the solubility increases with the saturation pressure (Figure 7 (a)). In this case, a gas concentration of 11.3% was obtained for 5.5 MPa, 15.6% for 10 MPa and finally 17.0% for 20 MPa. These data agree with the literature, where Miller et al.[26] show that increasing the saturation pressure increases the solubility value, sweeping pressures from 1 MPa to 5 MPa. In Figure 8, where the data obtained are plotted against those of Miller et al., it can again be seen that as the saturation pressure increases, the solubility increases, there being an apparently trend between all the data.

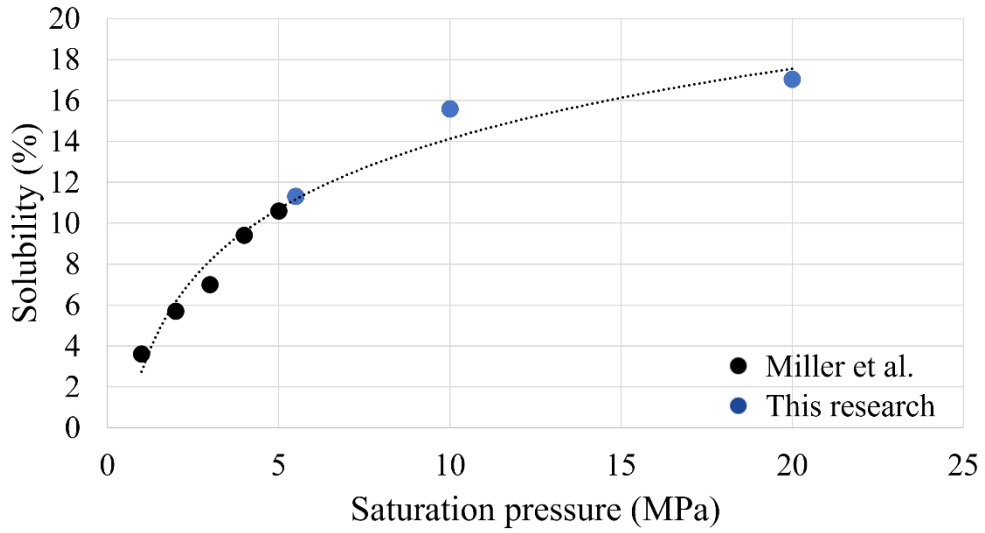

Figure 8. Solubility of PEI from this work as a function of saturation pressure at 24 ºC compared to Miller's results.

To compare the dependence on saturation pressure there are different models. The most common are Henry's model, Langmuir's model and the Dual model[33], which are represented graphically as shown in Figure 9.

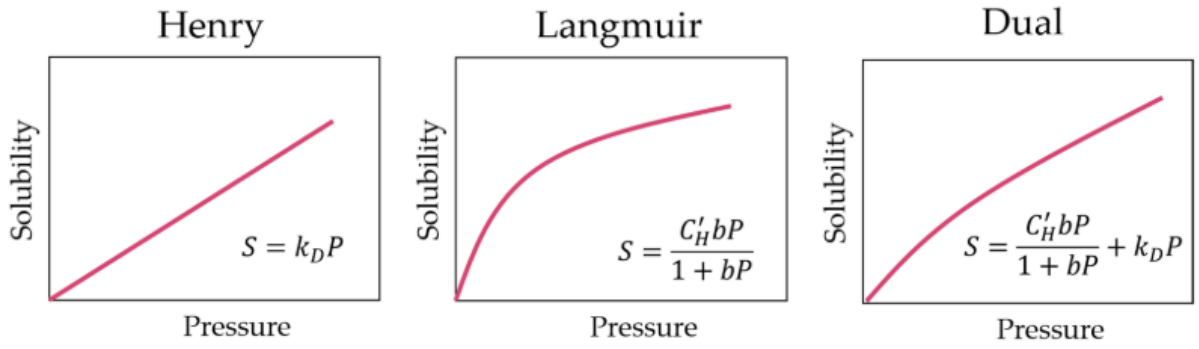

Figure 9. Graphical representation of the different models that study the dependence of solubility on saturation pressure.

As it can be seen in Figure 9, the Henry model is the simplest model as it predicts a linear dependence with pressure, but looking at the trend of the data, a better fit can be claimed for the Langmuir or Dual model. In Figure 10, we wanted to represent how the data fit the Langmuir model. This fit has been performed using the least squares method.

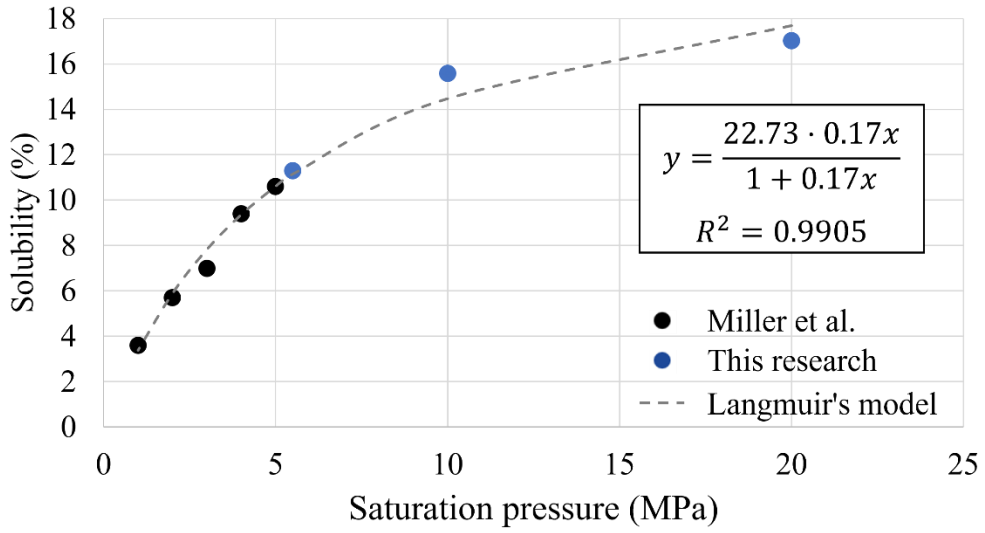

Figure 10. Solubility of PEI from this work as a function of saturation pressure at 24 °C compared to Miller's results and fitted to the Langmuir model.

For this work we have used the highest saturation pressures found in the literature, as Miller et al. reached a maximum of 5 MPa. Moreover, the solubilities obtained seem to be enough to reach nanometric cell sizes.

On the other hand, when the saturation pressure is kept constant (5.5 MPa), the solubility increases as the saturation temperature decreases (Figure 7 (b)). At 24 ºC a CO_2 concentration of 11.3% is obtained again, at 0 ºC, 16.4% and finally at -10 ºC up to 18.0%. This trend is also correct according to the Arrhenius equation[23], expressed in the equation (4).

$$S = S_0 \exp\left(-\frac{\Delta H_s}{RT_{Sat}}\right) \quad (4)$$

Where S_0 is the preexponential factor, ΔHs is the heat of sorption and R is the gas constant. For ΔHs <0, solubility increases with decreasing saturation temperature. The highest solubility obtained in the different samples was for the saturation conditions of -10 ºC and 5.5 MPa.

3.1.2. Precursor structure

To compare the cellular structure of the resulting materials with the solid precursor, Figure 11 shows the internal structure of the precursor material. As it can be seen, there are no cells, resulting in a completely solid and homogeneous material after the compression moulding process.

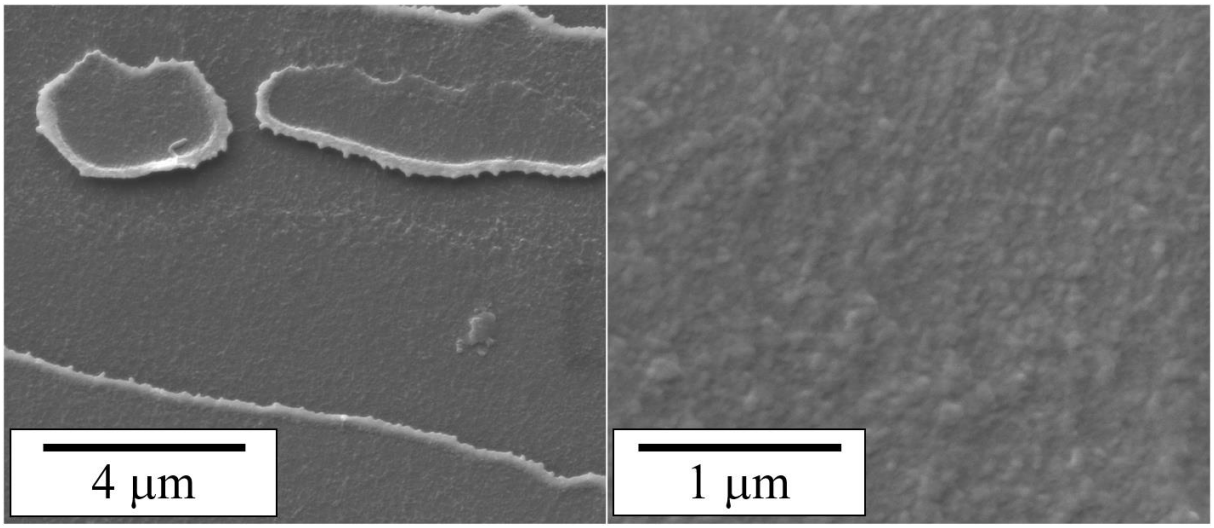

Figure 11. SEM micrograph of the PEI solid precursor at two magnifications.

3.2. Nanocellular materials

3.2.1. Relative density

Figure 12 shows that the relative density hardly changes regardless of the obtained solubility, and therefore on the used saturation conditions, obtaining in all cases a weight reduction of about 30%. If we compare these results with those obtained by Miller et al.[26] we can see that for cell sizes of 30 nm their samples show a relative density of about 0.7. In this case, the values obtained are very similar to those of Miller et al.

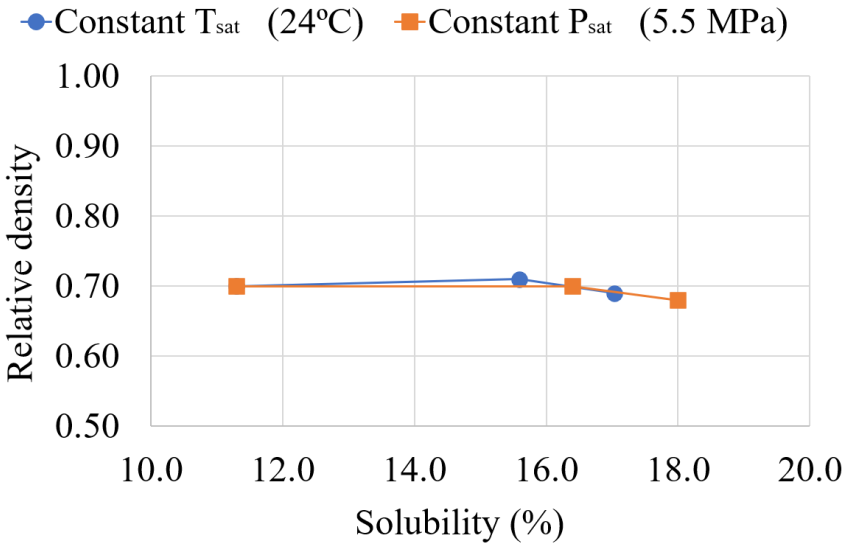

Figure 12. Relative density as a function of solubility for different saturation conditions.

3.2.2. Cellular Structure

Figure 13 shows the SEM micrographs of the cell structures obtained at constant saturation temperature (24 °C) and constant saturation pressure (5.5 MPa). As it can be seen, homogeneous structures with very small cell sizes have been obtained, with a reduction in the cell size as pressure increases and temperature decreases.

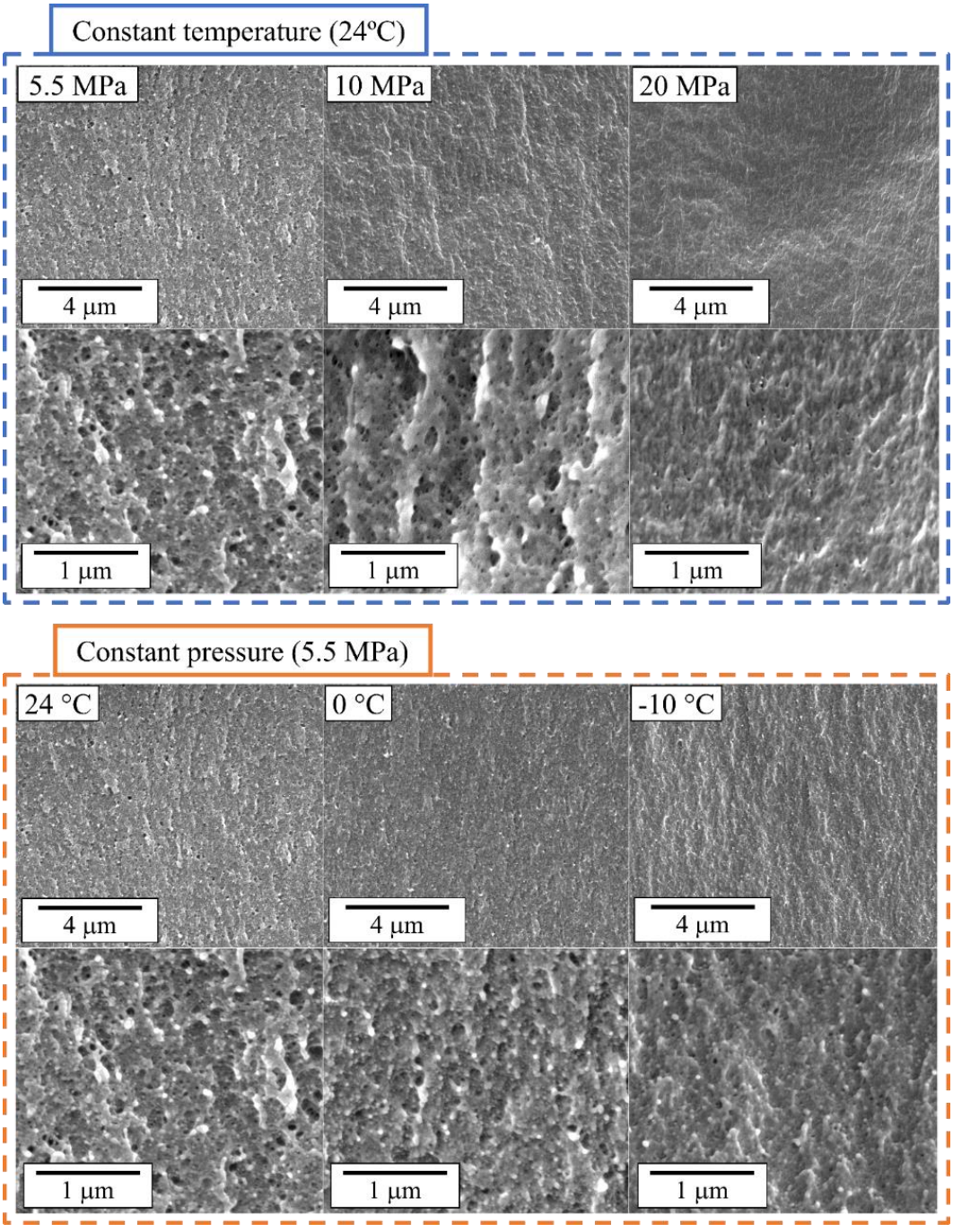

Figure 13. SEM images of nanocellular samples. The second raw corresponds to higher magnification images.

Figure 14 shows the cell size and cell nucleation density as a function of the solubility. If the samples saturated at constant temperature are observed, they show a significant reduction in cell size with increasing saturation pressure. For 5.5 MPa a cell size of 66 nm is obtained, but as we increase the saturation pressure, this is reduced getting 56 nm for 10 MPa and 45 nm for 20 MPa. As it can be seen from Figure 14 (a), an increase in the amount of gas absorbed from 11.3 to 17.0 wt% implies an increase in N_0 from 3.02×10^{15} to 9.42×10^{15} nuclei/cm^3. It can be seen from this graph that in order to decrease the cell size, nucleation needs to be increased. This is achieved by increasing the amount of CO_2 inside the sample.

On the other hand, in the samples saturated at constant pressure, a decrease in cell size is also observed with decreasing saturation temperature. For 24 ºC a cell size of 66 nm is obtained, but with decreasing saturation temperature, the cell size has been reduced to 39 nm for 0 ºC and -10 ºC. Figure 14 (b) shows again that in order to obtain smaller cell size values, it is necessary to increase the nucleation inside the sample. Furthermore, in this case, where a smaller cell size is obtained, the nucleation is higher for these samples than for the saturated samples at constant temperature.

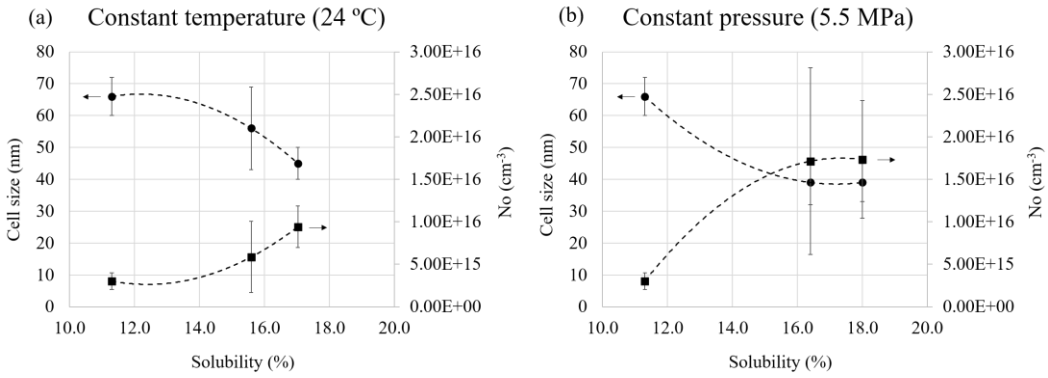

Figure 14. Cell sizes and nucleation versus solubility for constant saturation pressure (a) and for constant saturation temperature (b).

Moreover, all of data obtained are shown in Table 1. Although the samples were analysed using equation (1) where the number of cells per area is counted, there is a deviation in the results when several areas of the samples are measured. The low resolution of the images has forced us to use this method to estimate the size of the cells, which can give an error of between 10% and 20% in the measurement. These results are better verified in the transparency section. Finally, the SD/ϕ ratio is higher for samples with a larger cell size distribution, such as the sample saturated at 24ºC and 10 MPa. On the contrary, we find very homogeneous samples in the case of the samples saturated at 24ºC, 20 MPa and -10ºC, 5.5 MPa. Although all values are below 0.25, so the samples are generally quite homogeneous. It is

important to have homogeneous samples because this way the light has fewer obstacles to pass through the sample, thus increasing the transparency.

Table 1. Saturation conditions, cell nucleation density, cell size, SD and SD/Φ of the samples.

T_{Sat} (ºC)	P_{Sat} (MPa)	N_0 (nuclei/cm^3)	ϕ (nm)	SD (nm)	SD / ϕ
24	20	9.42×10^{15}	45	5	0.11
24	10	5.86×10^{15}	56	13	0.23
24	5.5	3.02×10^{15}	66	6	0.15
0	5.5	1.71×10^{16}	39	7	0.18
-10	5.5	1.73×10^{16}	39	6	0.09

3.2.3. Transparency

As it can be seen in the picture of Figure 15, PEI-based nanocellular samples have been obtained. Some of these samples show transparency. This macroscopic property can be affected by several factors, as previously explained, the cell size and the wavelength of the light passing through the sample. For this reason, a more comprehensive analysis of these parameters will be carried out.

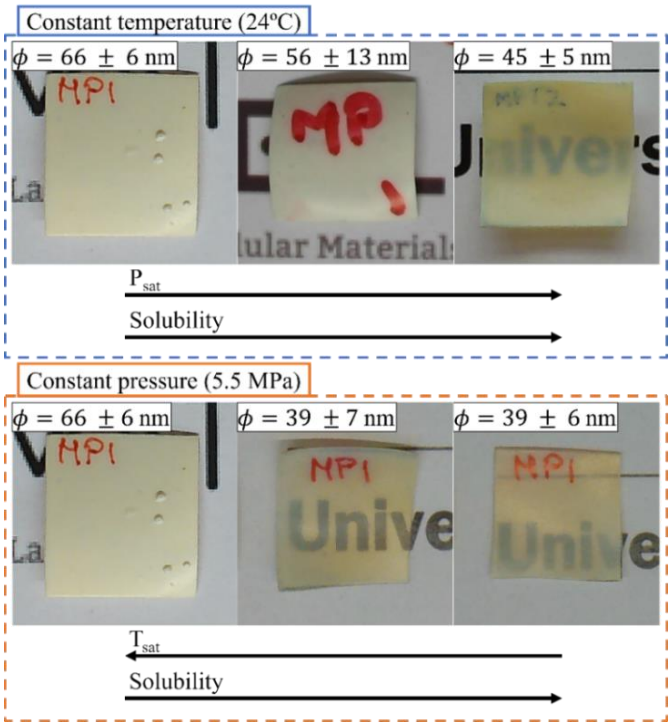

Figure 15. Nanocellular PEI samples.

3.2.3.1. Cell size dependence

The normalised transmittance (T_n) for samples with different cell sizes and for different wavelengths are shown in Figure 16.

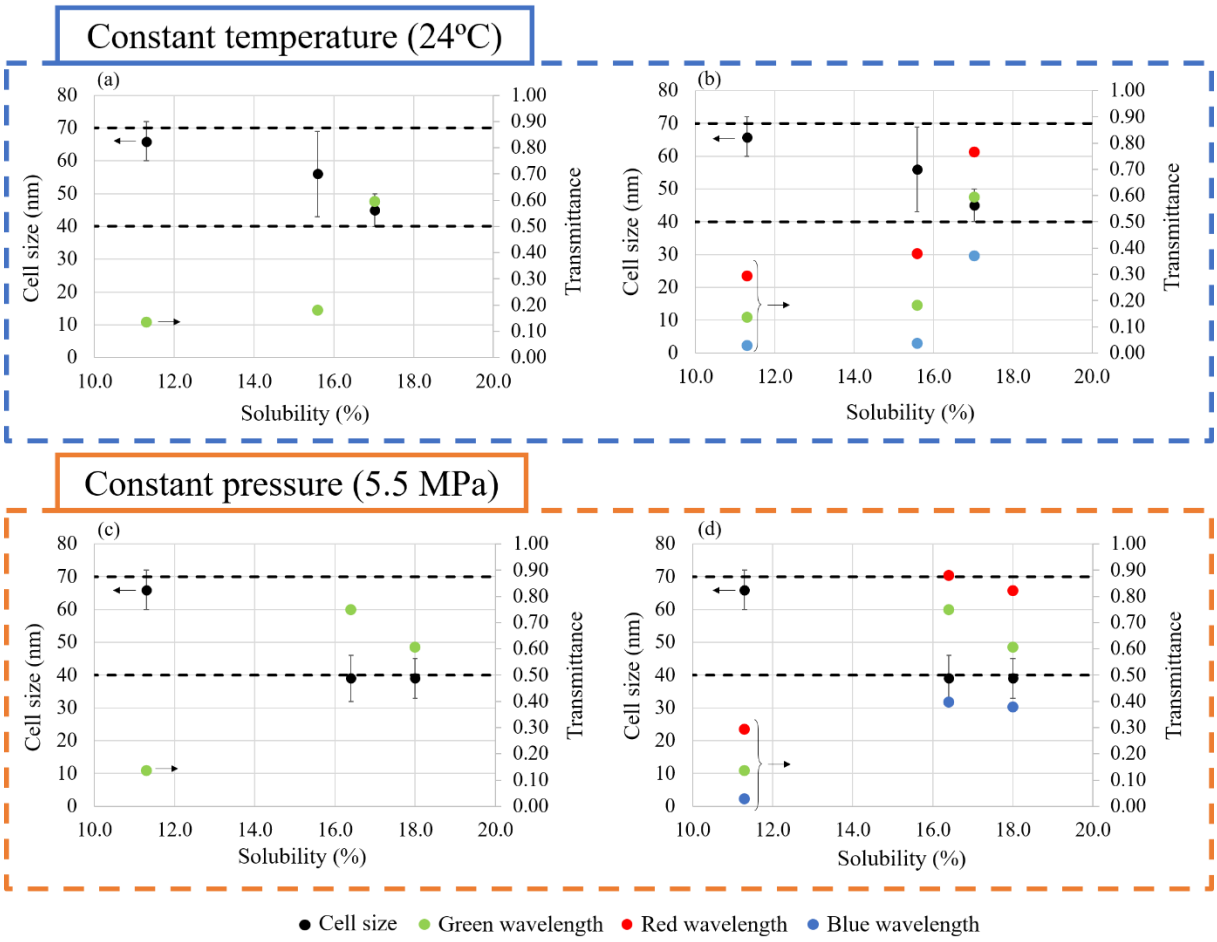

Figure 16. Cell size and transmittance of the samples versus solubility for constant saturation temperature ((a) for green colour only and (b) for all colours) and for constant saturation pressure ((c) for green colour only and (d) for all colours). The tenth part of the visible spectrum is indicated by the space between the dashed lines.

For the samples saturated at a constant temperature of 24°C, cell sizes of 45, 56 and 66 nm were obtained for 20, 10 and 5.5 MPa respectively. Figure 16 (a) represents cell size and green laser transmittance versus solubility. This representation allows one to see how cell size directly affects the transmittance of the samples. In addition, Figure 16 (b) represents the other measured wavelengths. With this characterisation of the materials, it is possible to make assumptions about the cell size distribution, which the SEM technique cannot observe due to the technical difficulties presented by this polymer. In the case of the sample saturated at 20 MPa with a solubility of 17.0%, values of 0.77 were obtained for the red wavelength, 0.59 for green and, finally, 0.37 for blue. These values indicate the presence of cells

smaller than 45 nm, as the blue colour can pass through the sample. On the other hand, samples saturated at 10 and 5.5 MPa, with solubilities of 15.6% and 11.3% respectively, show lower transmittance values. For red, values of 0.38 and 0.29 were obtained for 10 and 5.5 MPa, respectively. For green, the values were 0.18 and 0.14, and finally, for blue, the values were 0.04 and 0.03. These results confirm the presence of a significant number of cells above 45 nm, which means that it is impossible for the blue colour to pass through the sample. In addition, lower transmittance values for the red colour indicate the presence of cells above 65 nm.

In addition, for the samples saturated at a constant pressure of 5.5 MPa, cell sizes of 66, 39 and again 39 nm were obtained for 24, 0 and -10 °C respectively. The transmittances of the latter two samples are very similar. For the red wavelength, values close to 0.90 were obtained, while for green, they were about 0.70. Finally, for blue, values of about 0.40 were obtained. This means that both samples have many cells below 65 nm, which favour the passage of red light, but also have a significant number below 45 nm, as indicated by the high transmittance values for blue.

Although the change in cell size is small, it is in an important range since, as mentioned above, the maximum cell size to obtain a transparent polymer according to scattering theories is 50 nm[17]. Again, Figure 15 shows how this change in cell size can affect the macroscopic properties. Samples produced at 0 °C and -10 °C with smaller cell sizes show better transparency than samples with larger cell sizes, such as those produced at 24 °C under the same saturation pressure of 5.5 MPa. This is because samples saturated at lower temperatures acquire higher solubility, which leads to higher nucleation in the material and results in smaller cells. These results are consistent with the previous ones, since for the same saturation pressure, higher solubility is obtained as the saturation temperature decreases.

This trend is also repeated for samples prepared at the same saturation temperature of 24 °C, as can also be seen in Figure 15, where samples with higher solubility, such as the ones prepared at 20 MPa, obtain a smaller cell size than those prepared at 5.5 MPa. The value for the sample prepared at 10 MPa also yields an intermediate result, as expected. In this case, we also obtain consistent results regarding solubility values because when we produce materials at the same saturation temperature, the gas concentration inside the sample increases as the saturation pressure increases.

3.2.3.2. Wavelength dependence

As the transmittance has been measured for different colours, it is possible to study the transmittance of the samples as a function of the wavelength of the laser passing through the material. As it can be seen in Figure 16, the change in transmittance due to wavelength is strong. Larger wavelengths such as red

pass through the sample more easily than smaller wavelengths such as blue. This effect has previously been observed in various studies on PMMA[17,18,24], where these materials show similar characteristics to those studied in this work based on PEI. In these studies, the light scattering is associated with the scattering effects described by Rayleigh. As mentioned above, this phenomenon occurs when light interacts with objects smaller than one tenth of the wavelength passing through the material. According to this law, the transmittance can be calculated as described in equation (5):

$$T = Ae^{-\frac{Bl}{\lambda^4}} \tag{5}$$

Where A and B are constants. This exponential relationship can be transformed by the application of logarithms into a linear relationship as expressed in the equation (6).

$$-Ln(T) = \frac{Bl}{\lambda^4} - Ln(A) \tag{6}$$

In this way, when the -Ln(T) data are plotted as a function of l/λ^4, a straight line can be observed for all samples as it can be seen in Figure 17. This means that the nanocellular PEI samples prepared for this work exhibit Rayleigh scattering as previously demonstrated for nanocellular PMMA[17].

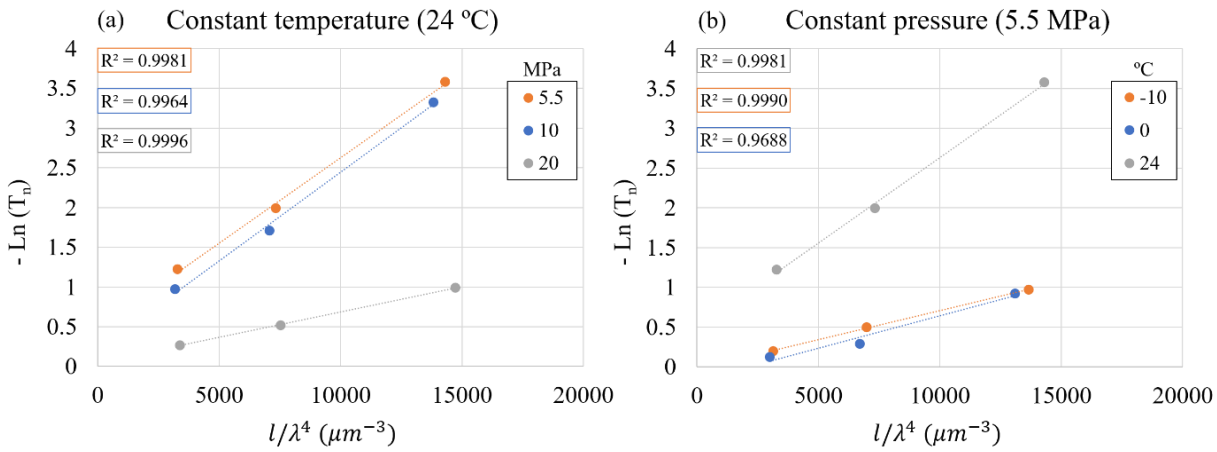

Figure 17. Representation of the linear dependence shown in equation (6). *(a) the saturated samples at constant temperature and (b) the saturated samples at constant pressure.*

As a final remark, in this work materials of transparent nanocellular PEI with cell sizes smaller than 50 nm were produced, achieving the goal of this research.

4. Conclusions

PEI-based transparent nanocellular materials have been obtained using the so-called *gas dissolution foaming* method.

On the one hand, nanocellular PEI has been produced with a constant saturation temperature of 24 ºC and three different saturation pressures of 5.5, 10 and 20 MPa (the highest in literature). On the other hand, by keeping the pressure at a constant value of 5.5 MPa and three saturation temperatures: 24, 0 and -10 ºC. Under these conditions, solubility values ranging from 11% to 18% were obtained., with an increase in solubility as pressure increases or temperature decreases. The obtained solubilities lead to obtain samples with a constant relative density of 0.7 and cell sizes ranging from 39 to 66 nm. As solubility increases cell nucleation density increases, resulting in a decrease of the cell size and obtaining the cell size minimum value for a solubility of 18 % obtained at 20 MPa and -10 ºC.

The produced samples are proven to present transparency when the cell size is below 50 nm, with transmittance values between 0.75 to 0.90 for the red wavelength for samples with the smallest cell size and a thickness of 0.5 mm. Values between 0.50 to 0.75, and 0.30 to 0.50 are obtained for green and blue wavelength respectively.

It has also been observed that the transmittance of these samples is highly dependent on the wavelength used. This dependence is specifically λ^{-4}, as predicted by Rayleigh scattering theories.

Moreover, a relationship has been established between the manufacturing processes of the materials obtained, the structure of the samples and the transmittance of the materials, thus establishing clear and precise conditions for the manufacture of nanocellular and transparent PEI.

Finally, after analysing all the results, the following objectives for future work are presented. The first is to explore different saturation and foaming processes to improve the transparency of the PEI samples. In addition, it would be interesting to obtain transparent samples for larger thickness sizes. Lastly, to extend this research to other high-performance polymers in order to obtain a homogeneous nanocellular structure leading to transparency.

5. Bibliography

1. Coreño-Alonso J, Méndez-Bautista MT. Relación estructura-propiedades de polímeros. *Educ Química*. 2010;21(4):291-299. doi:10.1016/S0187-893X(18)30098-3

2. Young RJ, Lovell PA. *Introduction to Polymers*. CRC Press; 2011. doi:10.1201/9781439894156

3. Coreño-Alonso J, Méndez-Bautista MT. Relación estructura-propiedades de polímeros. *Educ Química*. 2010;21(4):291-299. doi:10.1016/S0187-893X(18)30098-3

4. Fink JK. *High Performance Polymers*. Elsevier; 2014. doi:10.1016/C2013-0-18803-4

5. Hergenrother PM. The Use, Design, Synthesis, and Properties of High Performance/High Temperature Polymers: An Overview. *High Perform Polym*. 2003;15(1):3-45. doi:10.1177/095400830301500101

6. Martín de León J. Understanding the production process of nanocellular polymers based on pmma driven by a homogeneous nucleation. Published online 2019. doi:10.35376/10324/39466

7. Bernardo García V. Production and characterization of nanocellular polymers based on nanostructured PMMA blends and PMMA nanocomposites. Published online 2019. doi:10.35376/10324/37864

8. Okolieocha C, Raps D, Subramaniam K, Altstädt V. Microcellular to nanocellular polymer foams: Progress (2004–2015) and future directions – A review. *Eur Polym J*. 2015;73:500-519. doi:10.1016/j.eurpolymj.2015.11.001

9. Presas-Mata M. Comportamiento mecánico de materiales celulares de carburo de silicio. *Univ Politécnica Madrid*. Published online 2008.

10. Forest C, Chaumont P, Cassagnau P, Swoboda B, Sonntag P. Polymer nano-foams for insulating applications prepared from CO2 foaming. *Prog Polym Sci*. 2015;41(C):122-145. doi:10.1016/j.progpolymsci.2014.07.001

11. Notario B, Pinto J, Solorzano E, de Saja JA, Dumon M, Rodríguez-Pérez MA. Experimental validation of the Knudsen effect in nanocellular polymeric foams. *Polymer (Guildf)*. 2015;56:57-67. doi:10.1016/j.polymer.2014.10.006

12. Bernardo V, Martin-de Leon J, Pinto J, Verdejo R, Rodriguez-Perez MA. Modeling the heat transfer by conduction of nanocellular polymers with bimodal cellular structures. *Polymer (Guildf)*. 2019;160:126-137. doi:10.1016/j.polymer.2018.11.047

13. Sánchez-Calderón I, Bernardo V, Martín-de-León J, Rodríguez-Pérez MÁ. Thermal conductivity of low-density micro-and nanocellular poly(methyl-methacrylate) (PMMA): Experimental and modeling. *Mater Des*. 2022;221. doi:10.1016/j.matdes.2022.110938

14. Pinto J, Notario B, Verdejo R, Dumon M, Costeux S, Rodriguez-Perez MA. Molecular confinement of solid and gaseous phases of self-standing bulk nanoporous polymers inducing enhanced and unexpected physical properties. *Polymer (Guildf)*. 2017;113:27-33. doi:10.1016/j.polymer.2017.02.046

15. Martín-de León J, Van Loock F, Bernardo V, Fleck NA, Rodríguez-Pérez MÁ. The influence of cell size on the mechanical properties of nanocellular PMMA. *Polymer (Guildf)*. 2019;181(June):121805. doi:10.1016/j.polymer.2019.121805

16. Miller D, Kumar V. Microcellular and nanocellular solid-state polyetherimide (PEI) foams using sub-critical carbon dioxide II. Tensile and impact properties. *Polymer (Guildf)*. 2011;52(13):2910-2919. doi:10.1016/j.polymer.2011.04.049

17. Martín-de León J, Pura JL, Bernardo V, Rodríguez-Pérez MÁ. Transparent nanocellular PMMA: Characterization and modeling of the optical properties. *Polymer (Guildf)*. 2019;170(February):16-23. doi:10.1016/j.polymer.2019.03.010

18. Martín-de León J, Jiménez M, Pura JL, Bernardo V, Rodriguez-Pérez MA. Easy-way production of highly transparent nanocellular polymers films. *Polymer (Guildf)*. 2021;236:124298. doi:10.1016/j.polymer.2021.124298

19. LU GQ, ZHAO XS. NANOPOROUS MATERIALS – AN OVERVIEW. In: *Nanoporous Materials : Proceedings of the 5th International Symposium, Vancouver, Canada, 25-28 May 2008*. ; 2004:1-13. doi:10.1142/9781860946561_0001

20. Kiefer J, Hilborn JG, Hedrick JL. Chemically induced phase separation: A new technique for the synthesis of macroporous epoxy networks. *Polymer (Guildf)*. 1996;37(25):5715-5725. doi:10.1016/S0032-3861(96)00436-3

21. Martini-vvedensky JE, Suh NP, Waldman FA. Microcellular closed cell foams and fabrication.pdf. https://www.freepatentsonline.com/4473665.html

22. Colton JS, Suh NP. The nucleation of microcellular thermoplastic foam with additives: Part II: Experimental results and discussion. *Polym Eng Sci*. 1987;27(7):493-499. doi:10.1002/pen.760270703

23. Guo H, Kumar V. Some thermodynamic and kinetic low-temperature properties of the PC-CO2 system and morphological characteristics of solid-state PC nanofoams produced with liquid CO2. *Polymer (Guildf)*. 2015;56:46-56. doi:10.1016/j.polymer.2014.09.061

24. Martín-de León J, Bernardo V, Rodríguez-Pérez MÁ. Key Production Parameters to Obtain Transparent Nanocellular PMMA. *Macromol Mater Eng*. 2017;302(12):3-7. doi:10.1002/mame.201700343

25. Bernardo V, Martin-de Leon J, Rodriguez-Perez MA. Anisotropy in nanocellular polymers promoted by the addition of needle-like sepiolites. *Polym Int*. 2019;68(6):1204-1214. doi:10.1002/pi.5813

26. Miller D, Chatchaisucha P, Kumar V. Microcellular and nanocellular solid-state polyetherimide (PEI) foams using sub-critical carbon dioxide I. Processing and structure. *Polymer (Guildf)*. 2009;50(23):5576-5584. doi:10.1016/j.polymer.2009.09.020

27. Merlet S, Marestin C, Schiets F, Romeyer O, Mercier R. Preparation and Characterization of Nanocellular Poly(phenylquinoxaline) Foams. A New Approach to Nanoporous High-Performance Polymers. *Macromolecules*. 2007;40(6):2070-2078. doi:10.1021/ma062259t

28. Guo H, Nicolae A, Kumar V. Solid-state microcellular and nanocellular polysulfone foams. *J Polym Sci Part B Polym Phys*. 2015;53(14):975-985. doi:10.1002/polb.23719

29. Relles HM. Synthesis and Properties of Polyetherimide Polymers. *Contemp Top Polym Sci*. 1984;5:261-279. doi:10.1007/978-1-4613-2759-2_11

30. Jiang S, Liao G, Xu D, et al. Mechanical properties analysis of polyetherimide parts fabricated by fused deposition modeling. *High Perform Polym*. 2019;31(1):97-106. doi:10.1177/0954008317752822

31. Johnson RO, Burlhis HS. Polyetherimide: a New High-Performance Thermoplastic Resin. *J Polym Sci Polym Symp*. 1983;143(70):129-143. doi:10.1002/polc.5070700111

32. Carroccio S, Puglisi C, Montaudo G. Thermal degradation mechanisms of polyetherimide investigated by direct pyrolysis mass spectrometry. *Am Chem Soc Polym Prepr Div Polym Chem*. 2000;41(1):684-685.

33. Crank J. *The Mathematics of Diffusion.*; 1975.

34. Tang M, Du TB, Chen YP. Sorption and diffusion of supercritical carbon dioxide in polycarbonate. *J Supercrit Fluids*. 2004;28(2-3):207-218. doi:10.1016/S0896-8446(03)00045-7

35. Pinto J, Solórzano E, Rodriguez-Perez MA, de Saja JA. Characterization of the cellular structure based on user-interactive image analysis procedures. *J Cell Plast*. 2013;49(6):555-575. doi:10.1177/0021955X13503847

36. Kumar V, Suh NP. A process for making microcellular thermoplastic parts. *Polym Eng Sci*. 1990;30(20):1323-1329. doi:10.1002/pen.760302010